Fault-related oceanic serpentinization in the Troodos ophiolite, Cyprus: Implications for a fossil oceanic core complex

Perach Nuriel [a,*], Yaron Katzir [a], Meir Abelson [b], John W. Valley [c], Alan Matthews [d],
Michael J. Spicuzza [c], Avner Ayalon [b]

[a] *Dept. of Geological and Environmental Sciences, Ben Gurion University of the Negev, Be'er Sheva 84105, Israel*
[b] *Geological Survey of Israel, 30 Malkhe Israel St., Jerusalem 95501, Israel*
[c] *Dept. of Geology and Geophysics, University of Wisconsin, Madison WI 53706, USA*
[d] *Institute of Earth Sciences, the Hebrew University of Jerusalem, Jerusalem 91904, Israel*

ARTICLE INFO

ABSTRACT

Ultramafic rocks are exposed at the core of a domal structure near a fossil ridge–transform intersection (RTI) in the Troodos ophiolite. A sequence of heavily serpentinized rocks occurs adjacent to a major axis–parallel fault, the Amiandos Fault (AF), which juxtaposes them against gabbro. Previously, serpentinization and faulting were not considered to be related to the Cretaceous ocean spreading history of the Troodos ophiolite, but instead were interpreted as associated with late, emplacement-related tectonics and diapirism. Unusually high $\delta^{18}O$ values previously measured in Troodos serpentine (Srp) supported this view. Here, petrographic and isotope tracers (δD, $\delta^{18}O$) of water–rock interaction are examined in three profiles across the AF to determine the spatial distribution, temperature, and the type of water involved in serpentinization in the Troodos RTI. Complete serpentinization, widespread chrysotile veining and very high $\delta^{18}O$ (Srp), 10.6 to 12.6‰, characterize the rocks along a 2.5 km long profile at the central part of the serpentinite exposure. Much lower $\delta^{18}O$(Srp) values, 4.6 to 6.6‰, were measured at the AF fault zone in the highly serpentinized 300 m–long northern profile. Hydrogen isotope ratios also spatially vary: from −70 to −86‰ and −57 to −75‰ in the central and northern profiles, respectively. The bimodal distribution of isotope ratios calls for two distinct serpentinization events: localized 'oceanic-type' hydrothermal (100–200 °C) alteration initiated by deep infiltration of seawater during seafloor spreading followed by pervasive 'ophiolite-type' low-temperature hydration and veining along the AF. Superposition of the two serpentinization events is evident at a third, 2 km long southernmost profile, where $\delta^{18}O$ (Srp) values decrease gradually from 10.7‰ 2 km away from the fault to 5.0‰ at the AF fault zone. Post-magmatic decrease of $\delta^{18}O$(plagioclase) in gabbros in the footwall of the AF and the apparent lack of amphibolitization suggest high-temperature, off-axis gabbro-water interaction and focused fluid flow to the lower crust through the AF zone. These observations suggest that the Amiandos fault was active during seafloor spreading, possibly operating as a detachment fault in a core complex structure, exhuming progressively deeper levels of the oceanic lithosphere. This scenario is supported by additional observations such as the proximity to RTI and association with highly-rotated blocks in the sheeted dikes.

© 2009 Elsevier B.V. All rights reserved.

1. Introduction

Serpentinites that are formed by the interaction of seawater and peridotites most commonly occur in spreading environments characterized by low magmatic activity. Serpentinites have been dredged at numerous sites in slow spreading ridges (Karson et al., 1987; Cannat, 1993; Cannat et al., 1995; Reston et al., 2002) and are particularly abundant at ridge–transform intersections (RTIs) in association with detachment fault surfaces of oceanic core complexes (Blackmann et al., 1998; Cann et al., 2001; Ildefonse et al., 2007).

Oceanic core complexes (OCCs) are massifs where deep-seated rocks, gabbros, serpentinites, or peridotites, were exhumed onto the sea floor (e.g. Escartin et al., 2008; Tucholke et al., 2008) by slip along a detachment fault that cuts through the whole oceanic lithosphere (e.g. Cann et al., 1997; Blackmann et al., 1998; deMartin et al., 2007; Escartin et al., 2008; Smith et al., 2008; Tucholke et al., 1998). OCCs form in RTIs of ultraslow- to intermediate-spreading centers (Cannat, 1996; Okino et al., 2004); at spreading rates less than 8 cm/year (Escartin et al., 2008) and as a result of spreading dominated by amagmatic extension where only 30%–50% of the total extension is accommodated by magmatic accretion (Tucholke et al., 2008). It has been shown that hydrothermal fluid flow may occur along the major detachment fault (deMartin et al., 2007; McCaig et al., 2007). Thus,

mineral assemblages along such faults may record the conditions of water–rock interaction during slip and consequent exhumation (MacLeod et al., 2002; Escartin et al., 2003; Andreani et al., 2007; McCaig et al., 2007; Boschi et al., 2008).

Ophiolites, on-land slabs of oceanic lithosphere, are a major source of information for tectonic and hydrothermal processes in mid-ocean ridges (Gregory and Taylor, 1981; Gillis and Roberts, 1999; Varga et al., 1999; Humphris and Cann, 2000). A unique exposure of a fossil oceanic ridge–transform intersection (RTI) is preserved in the central part of the Troodos ophiolite in Cyprus (Allerton, 1989; Hurst et al., 1990; MacLeod et al., 1990; Abelson et al., 2002; Granot et al., 2006). Within the Troodos RTI ultramafic rocks outcrop at the core of a domal structure and are heavily serpentinized adjacent to a major fault, the Amiandos Fault (AF; see Fig. 1), which juxtaposes mafic against ultramafic rocks. The serpentinized domain was considered to be unrelated to the Cretaceous oceanic spreading history of the Troodos ophiolite, but interpreted as the exposed part of an emplacement-related Pleistocene serpentine diapir (Gass, 1990). However, this idea

has not been supported by detailed field, geophysical and geochemical studies. Furthermore, the location of the highly-serpentinized ultramafics raises the suspicion that these rocks are tectonically related to the fossil RTI of Troodos (Hurst et al., 1990).

The present study aims to investigate the provenance of the Troodos serpentinites using stable isotope tracers. We further discuss the tectonic implications of our results, especially with respect to oceanic core-complexes.

1.1. Tectonic setting

The slice of Turonian oceanic crust preserved in the Troodos ophiolite displays many of the structural features characteristic of modern spreading centers (Fig. 1): (1) a well-developed dike complex defining N–S trending spreading axes (Varga and Moores, 1985); and (2) an E–W trending oceanic transform in the southern margin of the ophiolite (Simonian and Gass, 1978). This makes the Troodos ophiolite an ideal site for on-land exploration of oceanic ridge–transform
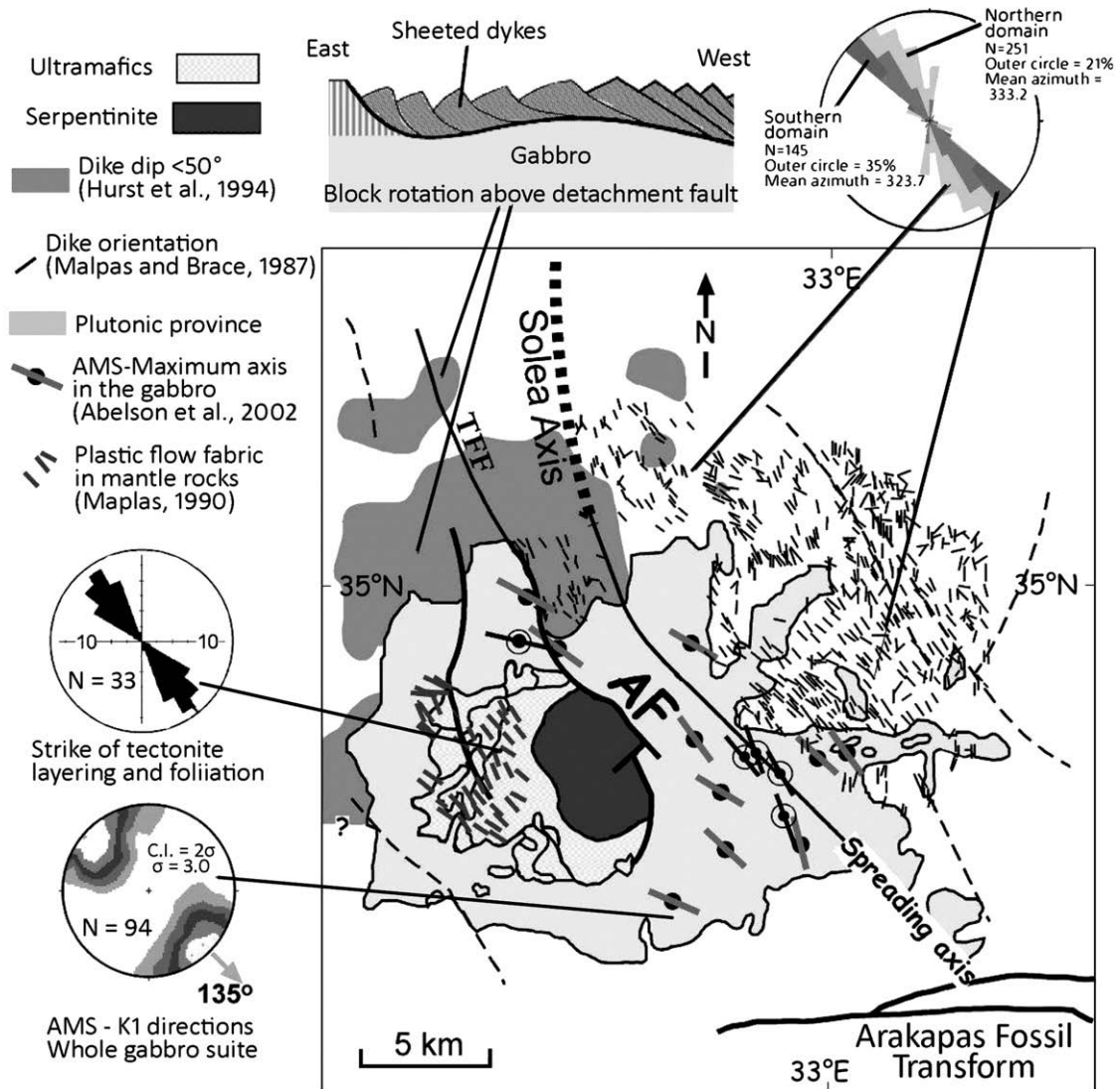
Fig. 1. The fossil ridge–transform intersection (RTI) between the Solea graben and the Arakapas transform (Abelson et al., 2002). The extinct spreading axis of the Solea graben is marked by a thick dashed line (Hurst et al., 1994) becoming a solid line through the gabbro suite (Abelson et al., 2002). Note that the axis curvature is compatible with a dextral transform. Structural features defining orientation of the extinct spreading axis are: (1) orientations of sheeted dikes (Hurst et al., 1994; Malpas and Brace, 1987); (2) orientations of tectonites representing plastic mantle flow (Malpas, 1990); (3) the Troodos Forest fault (TFF) that was active during seafloor spreading (Hurst et al., 1994), and (4) principal axes of magnetic susceptibility tensor (anisotropy of magnetic susceptibility–AMS) representing flow direction in axial magma chambers (Abelson et al., 2001). The southern continuation of the TFF, the Amiandos Fault (AF), juxtaposing mantle rocks against gabbros, is also parallel to the spreading axis. Dark gray areas represent domains of highly rotated blocks, dikes dip<50°, above a detachment fault (Hurst et al., 1994). Note that these domains are mainly associated with the mafic–ultramafic suites and are located west of the Solea axis.

intersections (RTI). However, until recently the geometry of the Troodos RTI was not fully understood: a plutonic complex composed of gabbros and ultramafics dwells between the palaeo-spreading center in the Solea graben and the fossil Arakapas transform and obscures the structure of the palaeo-axis, which is usually defined by sheeted dikes (Fig. 1). Magnetic and petrofabric studies in the gabbro suite traced the extinct spreading axis along a 20 km-long NW–SE trending segment, immediately to the south of the Solea graben (Abelson et al., 2001, 2002). The identification of the axis is supported by parallelism with other markers of axial deformation, including flow fabric within mantle rocks and orientation of dikes and major normal faults (Fig. 1). A major axis–parallel normal fault, the Troodos Forest Fault (TFF), hosts high-temperature hydrothermal mineralization and does not cut the overlying sediments. It is thus considered to have been active during seafloor spreading (Schiffman et al., 1987). Hurst et al. (1994) suggested that the TFF is a listric splay of a deep-seated detachment and that this fault accommodates the asymmetric extension observed in the Solea graben. The southerly extension of the TFF, the AF, juxtaposes heavily serpentinized ultramafics against gabbro. This fault has not been proven yet as active during seafloor spreading and therefore relations to the serpentinization are still ambiguous. However, the linkage between the TFF, which was active during seafloor spreading, and the AF demands examination whether the latter was active at spreading environment and how it was related to the serpentinites.

1.2. Timing and setting of serpentinization

Oxygen and hydrogen isotope studies, limited to a few locations within the highly serpentinized domain at the central part of Troodos ultramafic complex, mostly away from the TFF and AF, showed unexpectedly high $\delta^{18}O$ (Srp) values of 12.6 to 14.1‰ (Magaritz and Taylor, 1974). These values are different from those measured in ophiolite serpentines worldwide, which typically have $\delta^{18}O$ values of 5 to 9‰ (Wenner and Taylor, 1973; Agrinier et al., 1995). The water types and tectonic environment of serpentinization leading to the extremely high $\delta^{18}O$ values in the Troodos serpentinite are controversial. Magaritz and Taylor (1974) suggested that ^{18}O-enriched saline surface water and groundwater produced during the Messinian intense evaporation of the Mediterranean infiltrated downwards and serpentinized partially exhumed peridotites. Alternatively, Sheppard (1980) suggested that high-$\delta^{18}O$ brines associated with Messinian evaporites were released from an underthrust slab and interacted with the overlying mantle above a subduction zone located south of Cyprus during the Pleistocene. West of Mt. Olympus (see location in Fig. 2) another type of serpentine was described (Sheppard, 1980) in partially serpentinized harzburgites, dunites and pyroxenites exhibiting well-preserved igneous textures. $\delta^{18}O$ values of 4 to 5‰ in these western Troodos serpentinites (Sheppard, 1980), differ markedly from the central Troodos serpentinites measured by Magaritz and Taylor (1974). There are no temperature estimates for Troodos serpentinites,
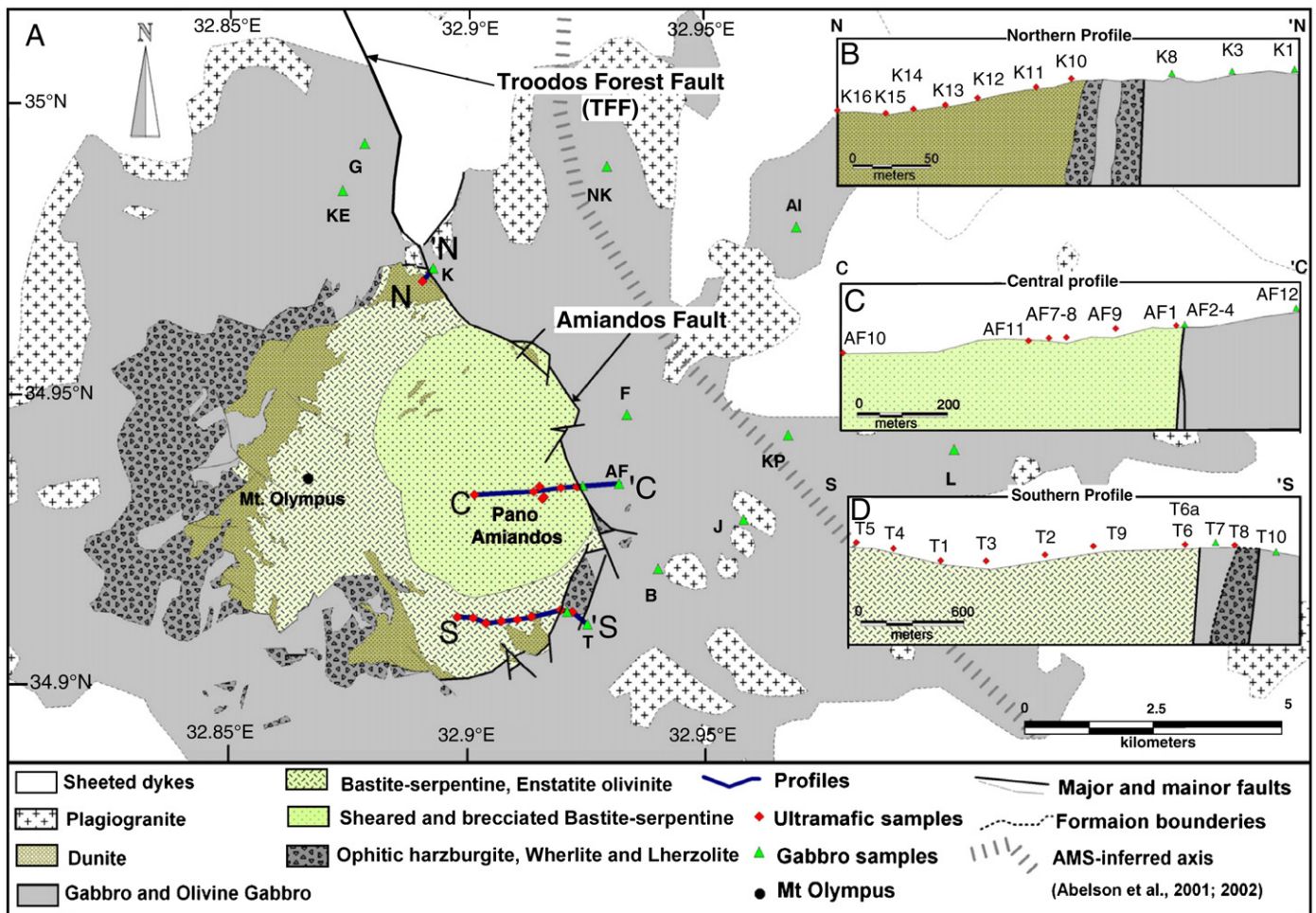

Fig. 2. Geological map of the central part of the Troodos massif (modified after Bishopp et al., 1978). (A) Locations of the northern, central and southern profiles are indicated as N–N, C–C and S–S, respectively. Note the different scale of the northern profile, only 300 m long, compared to the central and the southern profiles (2.5 and 3 km, respectively). Sampling sites within the gabbro suite are marked by triangles (Abelson et al., 2001, 2002). Major structures are also indicated: Troodos Forest Fault (TFF), Amiandos Fault (AF), and the inferred spreading axis (striped line); (B) schematic illustration of the northern profile and sample location within the profile, note the complexity of the magmatic lithology close to the fault zone; (C) the same for the central profile; (D) the same for the southern profile, note the igneous intrusive contacts versus Amiandos Fault offset contact.

and the two types of serpentine found in Troodos could have formed: (1) from isotopically similar waters at different temperatures; (2) from waters of different origin; or (3) by a combination of both. Currently, there is no explanation for the coexistence of two types of serpentine found in Troodos and the spatial distribution of these types is still unclear.

1.3. Hydrothermal alteration of the lower oceanic crust

Field relations in ophiolites and modern oceanic crust and the chemical composition of modern vent fluids place the base of the oceanic hydrothermal system near the sheeted dike–gabbro transition (Gillis, 1995; Bickle et al., 1998). While the recharge of seawater into the upper oceanic crust could be diffuse (Bickle et al., 1998) or more channelized (Malpas, 1990), the discharge fluids were clearly channelized through faults characterized by epidotization (Schiffman et al., 1987). However, petrological, stable isotope and fluid inclusion studies of Troodos massive gabbros indicate large influxes of fluids into the plutonic sequence (Heaton and Sheppard, 1977; Kelley and Robinson, 1990; Gillis and Roberts, 1999). Lowered $^{18}O/^{16}O$ ratios of amphibole in gabbros led Heaton and Sheppard (1977) to suggest large-scale hydrothermal cells circulating through a 3 to 5 km deep crust. This suggests deep penetration of seawater-derived fluids into the plutonic rocks of the Troodos RTI, possibly channeled through faults, as documented in oceanic gabbros of slow-spreading, magma-starved ridges (Mével et al., 1991). Alternatively, it is possible that the hydrothermal root zone migrated to significant depth in the plutonic sequence during the waning stages of magmatism (Gillis and Roberts, 1999). The petrological and geochemical study of the gabbros in the hanging wall of the AF can help understand the relations between hydrothermal alteration and tectonic exhumation of the lower crust at the Troodos ridge–transform intersection.

2. Analytical methods

Thin sections were examined under a polarized light microscope to study both the original magmatic and the secondary mineralogy. The degree of alteration was estimated from the modal fraction of hydrated minerals in both gabbros (mainly amphiboles) and ultramafic rocks (mainly serpentine). Rock-forming minerals in gabbro were handpicked based on the color and habit of crystals. Pure serpentine separates were produced by repetitive suspension of the fine ($<63 \mu$) non-magnetic fraction in an ultrasonic bath. The purity of the serpentine separates was confirmed by XRD.

Oxygen isotope analysis was performed by the laser fluorination technique at the University of Wisconsin-Madison, using a CO_2 laser, BrF_5 reagent and a Finnigan-MAT 251 mass spectrometer (Valley et al., 1995). Serpentine and plagioclase separates, which might react appreciably with BrF_5 at room temperature, were analyzed using an 'air-lock' sample chamber (Spicuzza et al., 1998). The measured oxygen isotope ratios were calibrated against the Gore Mt. Garnet standard (UWG-2) (Valley et al., 1995). On each day of analysis, 4–5 aliquots of UWG-2 were measured (± 0.1‰). Measured $\delta^{18}O$ values of serpentine and plagioclase were corrected by 0.32‰, on average, which corresponds to the difference of the accepted value of UWG-2 (5.8‰ VSMOW) from the average daily measured value. Similarly, amphibole and pyroxene sample analyses were corrected by 0.19‰ and 0.24‰, respectively.

Extraction of hydrogen from serpentine was performed in a vacuum line based on the zinc reduction method (Vennemann and O'Neil, 1993) at the Hebrew University of Jerusalem. Samples were reheated for an hour at 480 °C prior to isotope ratio analysis by mass-spectrometer in order to prevent hydrogen gas absorption by the zinc and fractionation during cooling (Demény, 1994). D/H ratios were measured on the SIRAII mass spectrometer at the Geological Survey of Israel. Analyses were corrected against NBS-30 biotite standard ($\delta D = -66$‰) and an internal

phengite standard (230 Mica) with measured difference of ΔD (230 Mica-NBS30) $= 17.3 \pm 2.3$‰ (Putlitz et al., 2000). The average standard value for 230 Mica during the serpentine analysis was -47.9 ± 6‰ ($n = 7$), within the accepted δD (230 Mica) $= -48.7 \pm 2.3$‰ range.

3. Results

Samples of gabbro and serpentinized peridotites have been systematically collected along three profiles that cross roughly perpendicular to the AF (Fig. 2). Representative samples of the Troodos gabbro suite, mostly east of the AF, including two samples west of the northern extension of the AF (sample KE and G in Fig. 2A) were also collected.

Brief petrographical descriptions and isotope ratios of all samples from this study are given in Table 1 (serpentinites) and Table 2 (gabbros). Representative micrographs of common textures in serpentinites are shown in Fig. 3 and variations of $\delta^{18}O$ and δD values of serpentine (Srp) with respect to the distance from AF zone in the three studied profiles are presented in Fig. 4.

3.1. Central profile

The central profile extends along 1.8 km at the central part of the highly serpentinized domain of Troodos (Fig. 2). The ultramafic protoliths are harzburgite and lherzolite and mafic plutonic rock compositions range from gabbro to olivine gabbronorite. The central profile fault zone includes major and secondary fault planes (Fig. 2C) and extremely altered serpentinite and gabbro (Fig. 3).

The most abundant textural type in the serpentinites of the central profile is mesh textured serpentine developed at the expense of olivine and serpentine bastite pseudomorphs after pyroxene. Both serpentine textural types are known to mostly consist of lizardite (Wicks and Whittaker, 1977). Up to 5 cm thick chrysotile veins are conspicuous in the field and in some outcrops compose up to 25–30% by volume. In thin sections of highly-veined samples, mesh-textured serpentine, though recognizable, is intensively overprinted by later generations of fibrous serpentine veins (Fig. 3A) and samples in general are highly altered (Table 1). It is thus not surprising that the former Pano-Amiandos asbestos mine was located within the area of the central profile. Gabbros of the central profile are strongly altered as evident by uralitized pyroxenes and the high modal amounts of secondary actinolite and hornblende (Table 2).

The $\delta^{18}O$(Srp) values of six samples from the central profile range from 10.6 to 12.6‰; among the highest $\delta^{18}O$ values measured in ophiolite serpentine and only slightly lower than the 12.6 to 14.1‰ $\delta^{18}O$(Srp) range measured in Troodos by Magaritz and Taylor (1974). The $\delta^{18}O$ values of three chrysotile veins from the central profile are 1–2‰ higher than the whole-rock serpentine of the same samples. The δD values of the central profile samples range from -70 to -87‰, and there is no correlation between the isotopic ratios and the distance from the fault plane in the central profile. The $\delta^{18}O$ values in plagioclase from the central profile range from 5.15 to 5.49‰, with the exception of one sample that has an extreme value of 13.1‰. The $\delta^{18}O$ values of other minerals from the gabbros of the central profile are given in Table 2.

3.2. Northern profile

The northern profile is an order of magnitude shorter than the central profile, crosses one major fault plane (Fig. 2A), and shows a complex lithology in the vicinity of the fault zone. The lithology changes from almost pure dunite away from the fault to cumulate rocks, pyroxenites and altered wehrlites intruded by gabbro pegmatite closer to the fault plane (Fig. 2B).

Dunites of the northern profile show almost complete alteration to mesh-textured lizardite (90–100%) associated with secondary

Table 1
General description and $\delta^{18}O(Srp)$ and $\delta D(Srp)$ values of samples from this study.

Sample	$\delta^{18}O‰$ (SMOW)	$\delta D‰$ (SMOW)	Rock type	Alt %	Texture	Chr %	Mineralogy
AF-1	11.92	–	Harzburgite	100	dM + Ba	25	L>C,Ma, Chl
AF-1v	13.98	–	Vein	100	–	100	C
AF-7	10.79	$-70.5 \pm 2.3(2)$	Lherzolite	100	dM+Ba	10	L>C, Ma, Opx,Cpx
AF-7v	12.13	–	Vein	100	–	100	C, Ma, T
AF-8	11.35	$-86.8 \pm 6.4(2)$	Lherzolite	90	dM + Ba	20	L>C, Ma, Chl, Opx, Cpx
AF-9	10.60	$-79.9 \pm 0.9(2)$	Lherzolite	75	dM	20	L>C, Ma, Opx, Cpx, Ol
AF-10	12.55	$-73.7 \pm 1.3(2)$	Harzburgite	100	dM + Ba	30	L, C, Ba, Ma
AF-10v	13.54	–	Vein	100	–	100	C, Ma
AF-11	10.67	$-75.3 \pm 3.0(3)$	Harzburgite	100	dM + Ba	15	L>C, Ma
K-10	$6.59 \pm 0.04(2)$	-75.7	Dunite	100	M	10	L>C, Ma, Chr
K-11a	$5.49 \pm 0.01(2)$	$-69.6 \pm 5.9(2)$	Harzburgite	95	M + Ba	5	L>C, Ma, Chr, Ol, Opx
K-12	$5.56 \pm 0.18(3)$	$-68.4 \pm 10.4(2)$	Dunite	100	M	10	L>C, Ma, Chr
K-13	$4.60 \pm 0.07(2)$	$-75.2 \pm 1.6(2)$	Dunite	95	M	10	L>C, Ma, Chr, Ol
K-14	$5.32 \pm 0.04(2)$	-56.8	Dunite	95	M	5	L>C, Ma, Chr, Ol
K-15	5.66	$-61.3 \pm 3.8(3)$	Dunite	90	M	5	L>C, Ma, Chr, Ol
K-16	6.00	$-62.9 \pm 0.8(2)$	Dunite	90	M	–	L, Ma, Chr, Ol
T-1	10.69	$-64.7 \pm 2.2(2)$	Harzburgite	65	M	–	L, Ma, Ol, Opx
T-2	8.08	-60.6	Harzburgite	75	M + Ba	5	L>C, Ma, Ol, Opx
T-3	8.88	$65.5 \pm 0.35(2)$	Harzburgite	70	M + Ba	–	L, Ma, Ol, Opx
T-4	10.26	$-60.8 \pm 5.5(2)$	Harzburgite	45	M	–	L, Ma Ol, Opx
T-5	8.99	$-63.5 \pm 2.2(2)$	Olvine– Orthopyroxenite	30	M	–	L, Ma, Ol, Opx
T-6	4.99	$-60.8 \pm 1.2(2)$	Harzburgite	100	M + Ba	60	C>L,Ma
T-6a	6.71	$-61.2 \pm 2.0(2)$	Harzburgite	90	M	–	L, Ma, Chr, Ol, Opx
T-6V	4.88	–	Vein	100	–	–	C, Ma
T-8	5.04	$-51.7 \pm 4.7(2)$	Ophitic lherzolite	65	M	–	L, Ma, Ol, Opx, Am
T-9	7.32	$-75.2 \pm 1.6(2)$	Harzburgite	60	M	–	L, Ma, Ol, Opx, Cpx

$\delta^{18}O$ and δD are in permil (‰) compared to SMOW, numbers in parentheses refer to numbers of repeat analyses.
Abbreviations: Alt% = degree of alteration. Chr% = volume percentage of chrysotile veins in the sample. Texture: dM/M = disturbed/undisturbed mesh texture, Ba = bastite texture. Mineralogy: L = lyzardite, C = chrysotile, Ma = magnetite, Ol = olivine, Opx/Cpx = Ortho and Clino-pyroxene, Am = amphibole, Chr = chromite, Chl = chlorite, T = talk.

magnetite in variable amounts and textures. In some samples magnetite is concentrated along relict grain boundaries, while in others higher concentrations can be found within veins. Chrysotile veins are rarely observed in the field; however, the modal abundance of chrysotile veins in thin sections is ≤10% (Fig. 3B).

The $\delta^{18}O(Srp)$ and $\delta D(Srp)$ values measured in 7 samples from the northern profile are 4.6 to 6.6‰ and −57 to −76‰ respectively, and are significantly different from the measured values in the central profile.

Mafic plutonic samples from the northern profile are slightly altered (30%), and fresh gabbronorite was observed (samples K-3 and K-1, respectively; Table 2). Sericite alteration of plagioclase appears to be associated with carbonate veins, representing late low-temperature alteration and deformation (Fig. 3D). The $\delta^{18}O$ values in plagioclase from the northern profile are 6.20 and 6.56/7.29‰ (sample K-1 and K-3 respectively). The two, very different $\delta^{18}O$(plagioclase) values of sample K-3 may suggest $\delta^{18}O$ zoning.

Table 2
$\delta^{18}O$ of various minerals from the gabbro suite.

Sample	Degree of alteration %	$\delta^{18}O$ (SMOW)					Rock type
		Plagioclase	Hornblende	Actinolite	Orthopyroxene	Clinopyroxene	
Northern profile							
K-1	0	6.20			5.40	4.85	Medium grained gabbronorite
K-3	30	7.29,6.56			$5.45 \pm 0.04(2)$	4.83	Medium grained gabbronorite
Central profile							
AF-2	70	13.07					Fine grained gabbro
AF-3	90	5.15					Coarse grained gabbro
AF-4	95	5.48	5.77	4.84			Coarse grained gabbro
AF-12	85	5.29		4.73	5.22		Coarse grained olivine gabbronorite
Southern profile							
T-7	50	5.30		4.66			Fine grained ophitic gabbronorite
T-10	100	4.88					Coarse grained, ophitic gabbronorite
Sporadically collected gabbro samples							
NK	90	4.18		$3.28 \pm 0.03(2)$			Fine grained gabbro
KE	0	5.62			$5.34 \pm 0.12(2)$		Coarse grained gabbronorite
J	60	2.78		$2.13 \pm 0.15(2)$			Coarse grained gabbro
F	60	4.73	$4.30 \pm 0.03(2)$				Coarse grained gabbro
G	0	4.36				$4.56 \pm 0.01(2)$	Coarse grained gabbronorite
AI	60	5.31		$4.86 \pm 0.03(2)$			Medium grained gabbro
B	70	3.04		$2.77 \pm 0.06(2)$			Coarse grained gabbro
L	70	4.48	$5.06 \pm 0.01(2)$	$2.34 \pm 0.16(2)$			Coarse grained olivine gabbronorite
KP	90	4.21					Medium grained gabbro
Average		$5.0 \pm 1.0(15)$	$5.0 \pm 0.2(3)$	$3.7 \pm 1.2(8)$	$5.4 \pm 0.01(4)$	$4.8 \pm 0.01(4)$	

Gabbro samples from the Northern, Central and Southern profiles are indicated as K, AF and T, respectively.
Samples of the gabbro suite away from the fault area are also shown (for sampling sites see Fig 1). An average value for each mineral (number of samples in parentheses) is given at the bottom of the table. The degree of alteration was estimated by the modal fraction of secondary amphibole minerals in the gabbros.
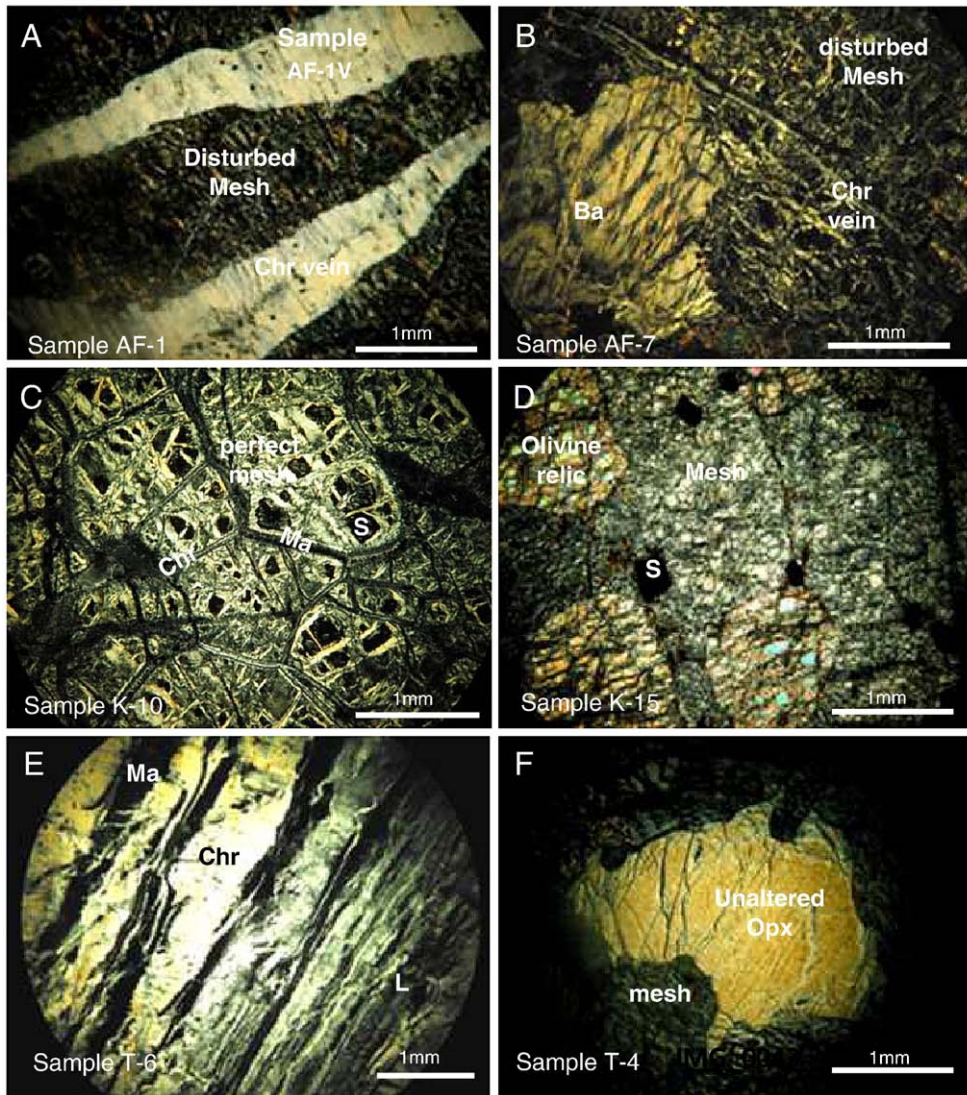
Fig. 3. Photomicrographs of Troodos serpentinites; XPL (A) Cross-fiber chrysotile vein (Chr vein) in disturbed mesh-textured lizardite (sample AF-1); (B) bastite plate (Ba) and chrysotile vein (Chr vein) in disturbed mesh-textured lizardite (sample AF-7); (C) magnetite (Ma) and chrysotile (Chr) concentrated along primary grain boundaries in a perfect lizardite mesh-texture, with idiomorphic mantle spinel (S) (sample K-10); (D) idiomorphic mantle spinel (S) in a partial mesh-textured lizardite with olivine relic (sample K-16); (E) magnetite (Ma) and chrysotile-rich (Chr) bands in lizardite serpentine (L) (sample T-6); (F) unaltered orthopyroxene (Opx) in a mesh-textured lizardite (Sample T-4).

3.3. Southern profile

The southernmost profile fault zone extends along 500 m and includes two main fault planes that juxtapose ultramafic rocks against mafic plutonic rocks; going eastwards one crosses serpentinized harzburgite, gabbronorite, serpentinized ophitic lherzolite and back to gabbronorite (Fig. 2D). This lithological sequence reflects superposition of igneous intrusive contacts and offsets by the AF (Schiffman et al., 1987).

Relict olivine and pyroxene are abundant in samples of the southern profile; igneous textures are generally preserved, and most pyroxene crystals are unaltered. The greater resistance to hydrous alteration of pyroxene relative to olivine is well known from ophiolites and oceanic peridotites (Mével, 2003). It follows that the fresh pyroxene-bearing serpentinites of the southern profile suffered less intense serpentinization compared to the bastite-bearing serpentinites of the central profile. Mafic rocks along the southern profile are altered; however, in the fault zone alteration is relatively low (T-7, 50%). Further to the east, gabbro is completely altered (sample T-10, 100%; Table 2).

The southernmost profile shows a gradual change of the isotope ratios towards the AF (Fig. 4). 1.5 km away from the fault $\delta^{18}O(Srp)$ and $\delta D(Srp)$ values are 10.7‰ and -75.6‰, respectively; at the fault zone, these values are 4.99‰ and -60.8‰. The $\delta^{18}O$ values in plagioclase from the southern profile are 5.30 and 4.88‰ and one actinolite sample gave $\delta^{18}O$ (Act) $=4.66$‰ (Table 2).

4. Discussion

4.1. Sequential serpentinization events in Troodos

Lizardite and chrysotile are the dominant mineralogical constituents of the Troodos serpentinites. Antigorite, the high temperature polymorph of serpentine, was not identified by petrographic inspection or by XRD in any of the studied samples. This observation suggests that the temperature of serpentinization in Troodos was not higher than ~250 to 300 °C (Evans et al., 1976). However the mineralogical and textural differences between serpentinites in the three sampling profiles are significant. The central profile serpentinites contain many more chrysotile veins and less mesh textured
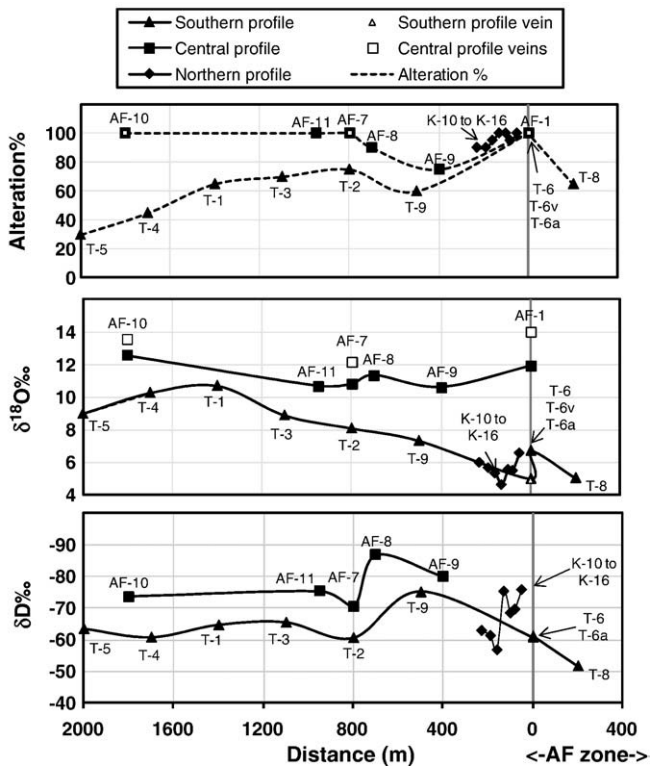
Fig. 4. Degree of alteration, $\delta^{18}O$ and δD values of serpentinites from the three studied profiles vs. distance from the fault zone. (A) Degree of alteration in the three profiles (solid symbols) (B) $\delta^{18}O(Srp)$ of samples from the three profiles (solid symbols) is shown together with $\delta^{18}O(Srp)$ values of chrysotile veins (open symbols). (C) $\delta D(Srp)$ of samples from the three profiles. Note that the northern profile is only 300 m long (diamonds). The gradual decrease in oxygen isotope ratios approaching the AF fault zone in the southern profile (triangles), stands in contrast to the high and relatively constant $\delta^{18}O$ values, along the central profile (squares). The $\delta^{18}O(Srp)$ values of the chrysotile veins from the central profile indicate that chrysotile is the major carrier of the high $\delta^{18}O$ signal. $\delta^{18}O$ and δD are in per mil (‰) SMOW.

serpentine compared to serpentinites of the other two profiles (Fig. 3A). Thus, sequential serpentinization events are recognized in the Troodos serpentinites. In the central profile, the latest, most dominant, event was the formation of the chrysotile veins. In contrast, the northern profile serpentinites mostly show undisturbed mesh-texture with scarce veining. This observation suggests an intense early serpentinization followed by minor vein formation. The southern profile shows fresh pyroxene-bearing serpentinites and has lower modal serpentine compared to the samples from the central and northern profiles. Petrographical examination does not support a number of hydrous alteration events, but rather, one relatively mild phase of serpentinization. However, approaching the AF, the degree of alteration increases dramatically (samples T-6, T-6a, T-6 V), suggesting intense serpentinization that was possibly related to fluid infiltration through the AF zone.

A number of simplified world-wide classifications of serpentinites have been published based on their sampling environment: oceanic versus ophiolitic serpentinite. Wenner and Taylor (1973) showed that these two types of serpentinite have distinct oxygen and hydrogen isotope signatures. Fig. 5 is a $\delta^{18}O(Srp)$–$\delta^{18}O(Srp)$ diagram for all the serpentinite samples from this study in which both isotope ratios were measured. The Troodos serpentinites form two clusters in Fig. 5. Samples from the central part of the serpentinite exposure lie at the uppermost extreme right part of the "ophiolite serpentinite" field, close to the values reported by Magaritz and Taylor (1974). Samples associated with the AF area, mostly from the northern profile, but also two samples from the southern profile, lie within or close to the "oceanic serpentinite" field. The rest of the samples from the southern

profile plot between these two 'end-member' groups and most likely represent superposition and mixing of two types of serpentinite, i.e. an 'oceanic serpentinite' type associated with AF area and the more regionally distributed 'ophiolite serpentinite' type.

Oxygen isotope overprinting occurs due to recrystallization of serpentine minerals and alteration of olivine and pyroxene relicts from former events, rather than due to isotope exchange (Wenner and Taylor, 1971). Since the serpentine–water fractionation is much larger at low temperature, an earlier record of high temperature serpentinization can be easily overprinted by even smaller-scale low temperature serpentinization. The $\delta^{18}O$ values of chrysotile veins from three samples along the central profile (AF-1, 7, 10) are consistently 1–2‰ higher than the $\delta^{18}O$ values of the whole-rock serpentine of the same samples. This suggests that the chrysotile veins formed at lower temperatures relative to their host serpentine, and since they cut all former textures (Fig. 3A), they represent the last, lowest-T serpentinization event. Chrysotile occurs, however, not only in separable veins, but also in micro-veinlets and as disseminated fibers in the host–rock matrix. The high $\delta^{18}O$ whole-rock values of serpentinites of the central profile thus most likely represent a mixture dominated by late chrysotile with subordinate former, lower-$\delta^{18}O$ relict mesh-textured serpentine. A nearly full obliteration of early, possibly oceanic serpentinites by late recrystallization and veining of 'ophiolite type' serpentine in a continental environment is recorded in the chrysotile-rich high-$\delta^{18}O$ serpentinites in the central profile. The obliteration of the early signature in the central profile, even within the AF zone, may suggest that the oceanic alteration at this locality along the fault was rather weak. However, if the degree of alteration was very high during early submarine serpentinization, especially in the vicinity of the fault infiltration area (McCaig et al.,
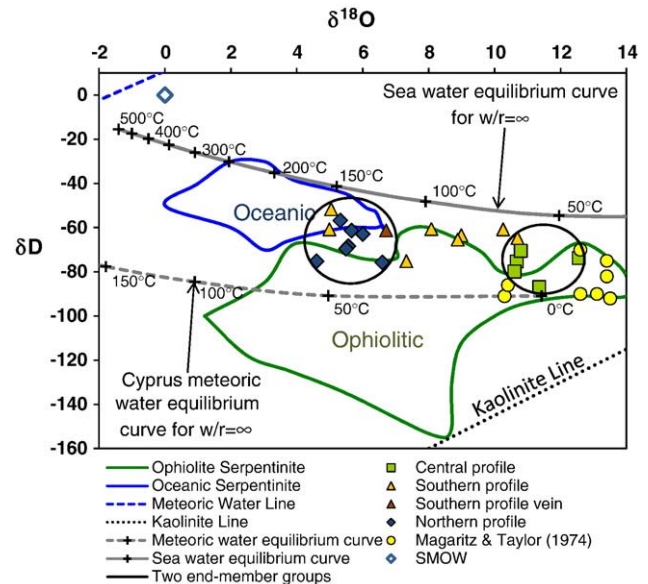
Fig. 5. $\delta D(Srp)$–$\delta^{18}O(Srp)$ diagram. The isotope ratios of Troodos serpentinites plotted on a δD–$\delta^{18}O$ diagram that shows the world-wide isotope fields of oceanic and ophiolite serpentinites (Wenner and Taylor, 1973; Agrinier et al., 1995). The position of the global meteoric water line (dashes) and kaolinite line (dots), as well as standard mean ocean water-SMOW (diamond), are also shown. Two end-member groups plotted as clusters around $\delta^{18}O = 10$–13‰ (central profile) and $\delta^{18}O = 4$–7‰ (northern profile and three samples from the southern profile fault zone). Most samples from the southern profile plot between these two end-members. The high-$\delta^{18}O$ cluster overlaps the values determined in Troodos serpentinites by Magaritz and Taylor (1974). The grey solid and dashed curves show the δD and $\delta^{18}O$ values of serpentine in equilibrium with sea water and Troodos meteoric waters, respectively, for a set of given temperatures (°C) calculated for w/r = ∞, using the serpentine–water fractionation equations for oxygen (O'Hanley, 1996) and hydrogen (Wenner and Taylor, 1973). Note that δD values of all samples plot between the seawater and meteoric water equilibrated values.

2007), an oceanic serpentine signature would be recorded. This is because only a minor amount of olivine would be left for replacement in the later serpentinization processes. Such a scenario is compatible with the fully serpentinized low-$\delta^{18}O$ mesh textured rocks of the northern profile and those adjacent to the AF in the southern profile. Moving away from the AF westwards along the southern profile the relative amount of oceanic serpentine gradually decreases in favor of progressively larger fractions of late, high-$\delta^{18}O$ serpentine that finally, at a distance of 1.4 km from the fault, completely dominates the rock (sample T-1, Fig. 4).

The combined isotope and petrographic evidence indicates that the Troodos ultramafic rocks were affected by two serpentinization events. The first event, characterized by ocean-like low $\delta^{18}O$ values, is mostly represented by mesh textured serpentine in the fault zone. A later, more regionally distributed overprint, highlighted in the central profile and involved with chrysotile vein formation, has high $\delta^{18}O$ values characteristic of serpentinization during ophiolite emplacement.

4.2. Late resetting of the hydrogen isotope ratios of Troodos serpentine

Fig. 5 also shows the $\delta D(Srp)$ and $\delta^{18}O(Srp)$ values of the Troodos serpentinites compared with the expected values of serpentine in equilibrium with seawater (~0‰), and Troodos meteoric water ($\delta D = -36.3$‰ and $\delta^{18}O = -7.0$‰, Boronina et al., 2005), at temperatures of 0° to 500 °C. These curves are calculated for infinite water/rock ratio (∞) using Wenner and Taylor (1971, 1973) fractionation factors for hydrogen and oxygen (modified by O'Hanley, 1996) isotopes between serpentine and water. The $\delta^{18}O(Srp)$ and $\delta D(Srp)$ values of the Troodos serpentine lie between the seawater and meteoric water equilibrium curves, thus implying post-formation partial exchange of hydrogen with the local meteoric waters. Magaritz and Taylor (1974) suggested that the δD values of the Troodos serpentine that they measured were lowered by 20–30‰ during the serpentinization process, either by diffusion or mixing. However, later hydrogen isotope studies presented strong evidence for post-formation hydrogen isotope exchange of geologically old lizardite–chrysotile serpentinites with waters that correspond to the correlation between δD of meteoric water and latitude (Kyser and Kerrich, 1991). This raises the possibility that the decrease in hydrogen isotope ratios seen in Troodos is also due to post-formation exchange with local meteoric waters. Lower w/r ratio could also produce the measured δD values of the serpentinites. However, given the relatively high degree of alteration observed in samples in which δD was measured, this is an unlikely explanation. While the measured $\delta D(Srp)$ in Troodos most probably does not preserve evidence of serpentinization events, the $\delta^{18}O$ values of the Troodos serpentinites can be used to estimate the temperature and the type of water involved in their formation.

4.3. Oxygen isotope constraints on water–serpentine interaction

In order to constrain the temperature and $\delta^{18}O(H_2O)$ during serpentinization at Troodos, a material balance calculation for open system conditions was performed. In a dynamic single-pass open system model (Taylor, 1977; Gregory et al., 1989) infinitesimal packets of water are progressively flushed through the system to interact completely with the rock and then leave the system. Since we consider that water–rock interaction in the AF zone in Troodos is essentially due to fluid infiltration in the fault zone, this model is preferred over other closed system (Wenner and Taylor, 1973; Sakai et al., 1990), reactive transport (e.g. Ferry, 1986) and time-integrated fluid flux (e.g. Dipple and Ferry, 1992) models. Calculations at very high water/rock ratio are essentially the same when using open and closed system models. However, when the water/rock ratio is reduced, the calculations become model-dependent. For this reason we used in our calculation $\delta^{18}O(Srp)$ of samples that have high modal fraction of serpentine minerals (90–100% alteration), indicating high w/r ratios

conditions. The water–serpentine oxygen isotope exchange is modeled within the temperature range of lizardite–chrysotile formation (0–300 °C) for two end-member w/r ratios (∞ and 1), assuming initial rock isotope ratio of 5.7‰ (Mattey et al., 1994) and using the serpentine–water fractionation equation of O'Hanley (1996). The temperature dependence of the $\delta^{18}O$ value of serpentine that equilibrated with water of variable initial isotope ratio is presented in Fig. 6. The $\delta^{18}O(Srp)$–T curves are shown for three representative initial $\delta^{18}O(water)$ compositions: -7‰ (Troodos meteoric water), 0‰ (seawater) and $+5$‰ (brine, ^{18}O-enriched aqueous fluid).

The isotope exchange model calculation indicates that the two types of Troodos serpentinite, which define the distinct $\delta^{18}O$-fields in Fig. 6, could not have formed coevally. The high $\delta^{18}O$ serpentinites had to form at much lower temperatures compared to the fault related serpentinite. This conclusion supports the view that at least two distinct serpentinization events are recorded in Troodos, and that it is most likely that the high-$\delta^{18}O$ serpentinization postdated the fault related serpentinization.

Fig. 6 shows that in order to form the fault-related serpentinites by interaction with high $\delta^{18}O$ fluids (either brines or burial metamorphic waters), the temperatures of hydration should have been as high as 275° and up to 450 °C. The upper stability field of lizardite is considered to overlap these temperatures (Evans et al., 1976), and since all of our samples from this study are lizardite, serpentinization by high-$\delta^{18}O$ water is unrealistic. Likewise meteoric water interaction at temperatures between 30–60 °C is also unlikely to account for the observed $\delta^{18}O$ values in the fault related serpentinites. If serpentinization processes had occurred only at a late continental setting, then the high-$\delta^{18}O$ serpentinites should have formed from the same water as the low-$\delta^{18}O$ ones and at reasonable near-surface temperatures, but not below zero as predicted for meteoric water in our model. In addition, δD values should have obeyed the correlation of δD and latitude (Kyser and Kerrich, 1991), but Fig. 5 shows that there is no such correlation and δD values most probably represent a mixture of values. The isotope composition of the fault related serpentinites resemble both $\delta^{18}O$ and δD values of oceanic serpentinites rather than those of the ophiolitic type.

Notwithstanding the above scenarios, current fluid temperatures within the Atlantis massif on the Mid-Atlantic Ridge under the Lost City reported to be at the range of 110–150 °C based on measured venting temperatures, temperatures calculated from $\delta^{18}O$ analysis (Kelley et al., 2005), and hydrogen isotope thermometry of the vent fluids (Proskurowski et al., 2006). Somewhat higher temperatures
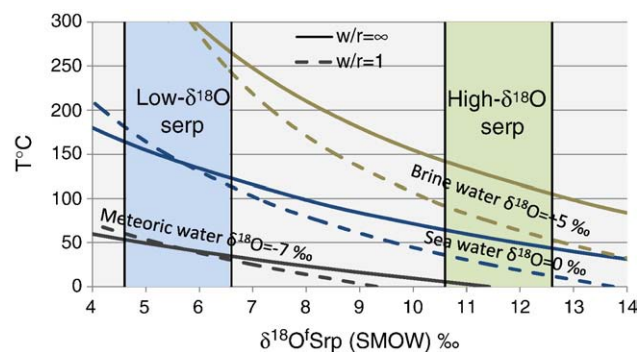

Fig. 6. Temperature vs. $\delta^{18}O(Srp)$ final curves showing the temperature-dependence of the calculated final oxygen isotope ratio of serpentine as a result of equilibrium water–serpentine interaction (O'Hanley, 1996), given variable water/serpentine ratios, (infinite and 1, filled and dashed curves respectively) and initial water compositions: 0‰ (seawater), -7‰ (Troodos meteoric water), and $+5$‰ (brine). Ranges of $\delta^{18}O$ values of the fault related serpentinites ($\delta^{18}O$ range between 4.6 and 6.6‰) and high-$\delta^{18}O$ serpentinites from the central profile ($\delta^{18}O$ range between 10.6–12.6‰) are also shown.

have been recorded in some basement samples, locally indicating paleotemperatures up to 185 °C (Früh-Green et al., 2003). Our oxygen exchange calculations (Fig. 6) show similar temperature range (110°–180 °C) for seawater–rock interaction in the Troodos fault-related serpentinites. We therefore suggest that the fault-related serpentinite formed by interaction with seawater at 110–180 °C, and most likely formed at a spreading environment.

The high-$\delta^{18}O$ serpentinites formed at much lower temperatures relative to the fault-related serpentinites (below 140 °C), regardless of the specific water type involved in their formation (Fig. 6). The type of water involved in the formation of the high-$\delta^{18}O$ serpentinites is more difficult to characterize. However, as argued above, it must have postdated the fault-related serpentinization, and the observation that these serpentinites are highly veined and mesh texture is not well preserved suggests that serpentinization occurred in an ophiolite emplacement tectonic environment. The complete serpentinization in the central profile suggests a very high w/r ratio. Slightly $\delta^{18}O$-elevated rainwater and groundwater (~0‰) could have formed these anomalously-high $\delta^{18}O$ serpentinites at near-surface temperatures (Magaritz and Taylor, 1974). Alternatively, high-$\delta^{18}O$ aqueous fluids, e.g. Messinian brines (Magaritz and Taylor, 1974), might have been involved in hydration of the Troodos ultramafic rocks at temperatures of 50–140 °C (Fig. 6).

4.4. On-axis and off-axis alteration of the Troodos gabbros

The gabbro suite of Troodos was sampled to test possible relations between hot hydrothermal fluids that circulated in the deep oceanic crust and lower temperature serpentinization of the exhumed peridotites. A δ–δ diagram showing the oxygen isotope fractionation of plagioclase against coexisting minerals is presented in Fig. 7. Using

the experimental plagioclase–clinopyroxene calibration of Matthews et al. (1983) a value of $\Delta^{18}O[Plg(An_{70})–Cpx] = 0.71‰$, retained from the time of magma crystallization (~800°) is expected. This is shown as a non-dashed isotherm line in Fig. 7. Equilibrium at lower temperatures would produce a linear trend above this line ($\Delta = 1.4‰$, dashed line in Fig. 7 for 500 °C). In Fig. 7, however, plagioclase-pyroxene pairs (squares) plot along a steeply dipping trend cutting the isotherms and implying isotope disequilibrium. While the magmatic $\delta^{18}O$ values of pyroxene are preserved, as indicated by high temperature $\Delta^{18}O(Opx–Cpx)$ values, plagioclase has either low-$\delta^{18}O$ (samples G, KE and AF-12) or high-$\delta^{18}O$ (K-1 and K-3) values relative to its magmatic equilibrium value. Since plagioclase is very sensitive to hydrothermal alteration, oxygen exchange with an external reservoir may occur more rapidly compared with fluid-pyroxene exchange. Thus, the steep Plg–Cpx trend suggests open-system isotope exchange with fluids as observed in many other hydrothermally altered plutonic rocks (Gregory and Taylor, 1981). However, hydrous metamorphic minerals (amphiboles), are completely absent in samples KE and G. The decrease in $\delta^{18}O(plagioclase)$, together with the absence of amphiboles, may suggest water–rock interaction at very high temperatures and low water/rock ratios (Stakes, 1991). Samples from the northern profile are somewhat altered (K-1 and K-3), but plagioclase has high-$\delta^{18}O$. Increase in $\delta^{18}O$ (plagioclase) accompanied with amphibolitization suggests lower temperatures of water–rock interaction, possibly reflecting a shallower location within the lower crust. It is noteworthy that the low-$\delta^{18}O$ (Plg) samples, G and KE, are located west of the northern extension of the AF (Fig. 2), whereas the high-$\delta^{18}O$ (Plg) samples, K-1 and K-3, outcrop east of the fault. Juxtaposition of a deeper western block against a shallower eastern one is consistent with the overall motion along the AF.

Unlike pyroxenes most of the plagioclase–amphibole pairs plot along the high temperature equilibrium ($\Delta = 0.7‰$) line [excluding sample L-20 with $\Delta^{18}O(Hornblende–Actinolite) = 2.7‰$, which might reflect disequilibrium; Kohn and Valley (1998)]. Under equilibrium conditions $\Delta^{18}O(Plg–Amph)$ is a function of temperature and independent of the isotope ratio of the fluid. The measured plagioclase–amphibole fractionations, ~0.7‰, plot along the 700 °C anorthite–tremolite isotherm that was calculated based on experimental calibrations with calcite (Clayton et al., 1989; Zheng et al., 1994). However, solid solution effects on oxygen isotope fractionations in both plagioclase and amphibole are large and hard to calibrate (Clayton et al., 1989; Kohn and Valley, 1998) and thus the linear Plg–Amph array may indicate equilibrium isotope exchange, but cannot accurately constrain the temperature of equilibration. Amphibolite facies temperatures (500–600 °C) are thus assumed for the crystallization of amphibole in Troodos gabbro (See Heaton and Sheppard, 1977).

The majority of the Plg–Amph pairs (triangles) are from samples mostly located away from the AF zone and within the 'extinct spreading axis' location (Abelson et al., 2002), excluding samples AF-4, 12, and T-7, which overlap with the Plg–Cpx trend. This high-temperature equilibrium trend of the Plg–Amph pairs could be associated with an on-axis hydrothermal alteration system. In contrast, the Plg–Cpx pairs (squares) are from samples that are mostly within the fault zone (samples K-1, K-3, KE, G and AF-12), and as mentioned above, their overall trend reflects open-system hydrothermal alteration that can be related to the off-axis location of the AF. The AF is shown here to play an important role in deep off-axis hydrothermal processes. This supports the observation from the ultramafic section that the ridge axis-parallel fault was active in an oceanic-spreading environment.

4.5. Tectonic implications — fossil oceanic core complex

A model for the tectonic evolution leading to the alteration and serpentinization processes in the Troodos massif is portrayed in Fig. 8.
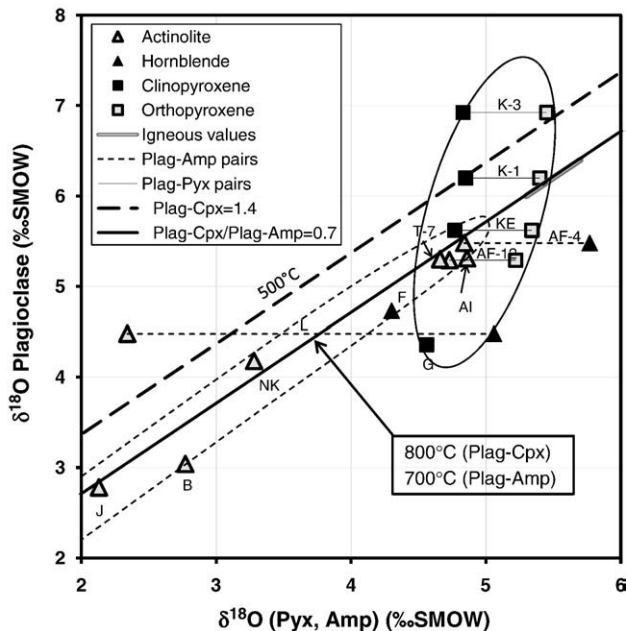

Fig. 7. Oxygen isotopic ratios of plagioclase and coexisting minerals in the Troodos gabbro suite. Plagioclase–pyroxene and plagioclase–amphibole pairs are shown by squares and triangles, respectively (amphiboles and pyroxenes from the same sample are joined by tie lines). Predicted fractionations for Δ(plagioclase–clinopyroxene) at $T = 800$ °C (solid), 500 °C (heavy dashed line), are calculated after Matthews et al. (1983), and Δ(plagioclase–Amphibole) at $T = 700$ °C (full line) is calculated after Clayton et al. (1989) and Zheng et al. (1994). Note that plagioclase–pyroxene pairs form a vertical array whereas plagioclase–amphibole pairs form an equilibrium array. Sample locations are shown in Fig. 2.
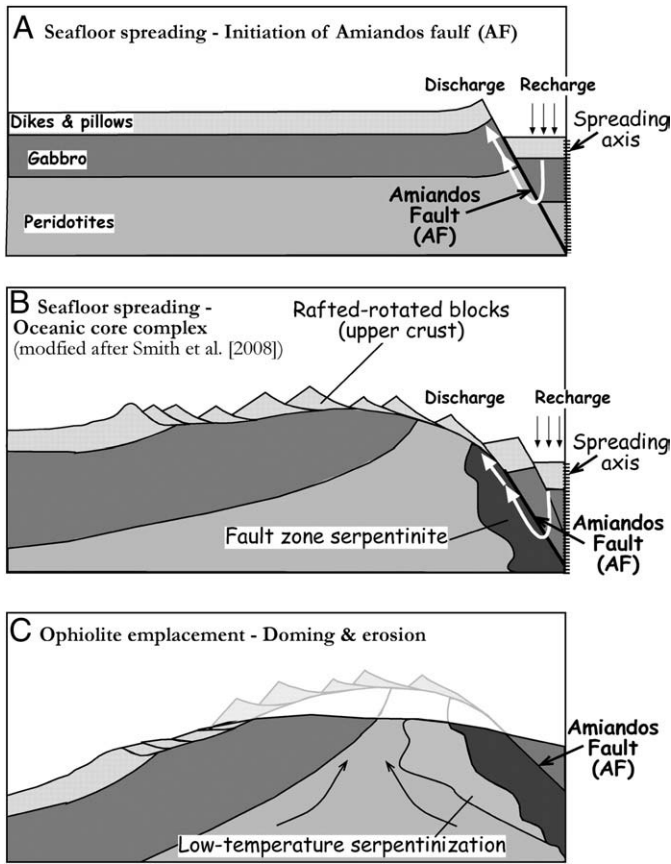
Fig. 8. Stages in the tectonic evolution and hydrothermal alteration of the fossil ridge transform intersection (RTI) in Troodos. (A) Initiation of the AF as major normal fault at the spreading axis during a phase of domination of tectonic- over magmatic-spreading at a segment edge. Recharge of seawater and near axis alteration of gabbro (lower crust) at high temperature (<500 °C). Prior to rotation, epidote formed in the upper crust by alteration assisted by hydrothermal discharge fluids at lower temperature (300°–370 °C) (Varga et al., 1999). (B) Continuation of tectonic spreading leading to rotation of main fault into a shallowly-dipping detachment fault underlying rotated blocks of sheeted dikes, i.e., rafted-blocks above detachment (Smith et al., 2008). Note that dissimilar to the Smith et al. (2008) model, rotated blocks in the upper crust are also found between the detachment fault splay (TFF) and the Solea paleo-spreading axis (Fig. 1), similarly found in other core complexes (Wernicke, 1992; Blackmann et al., 1998; Tucholke et al., 2001). This is likely to occur especially where the detachment fault in the upper ~1.5 km of the oceanic crust is flat (20°) as found in the TAG area, MAR (deMartin et al., 2007). Serpentinites were formed in the mantle rocks in the vicinity of the AF during and/or after block rotation. The exposed serpentinite was altered at shallow level ~2 km below seafloor by waters with temperatures of 100°–180 °C. (C) Doming during ophiolite emplacement is accompanied by low temperature serpentinization.

The observation that 'oceanic type' serpentinites are associated with the fault zone suggests that the AF served as a conduit for discharge of seawater circulating through the oceanic crust. Therefore, this fault has been active during the operation of the Troodos spreading center at the mid-Cretaceous (Fig. 8A). This finding is in agreement with previous suggestions that the TFF, the northerly extension of the AF (Fig. 1), was active during seafloor spreading (Hurst et al., 1994). These two faults were parallel to the extinct spreading axis as indicated by their parallelism with the strike of the adjacent dikes (Fig. 1), which mark the spreading axis orientation (e.g. Nicolas and Boudier, 1995). In addition, these faults are also parallel to other structural features related to the spreading axis including tectonite layering in the ultramafic rocks and magnetic fabric in the gabbro (Abelson et al., 2001, 2002) (Fig. 1). According to these findings, the oceanic crust west of the Solea extinct spreading axis comprises: (1) axis-parallel fault that juxtaposed gabbros against

ultramafic rocks during seafloor spreading; and (2) highly rotated blocks (dip<50°) in the upper crust (sheeted dikes). These observations, together with the location at the fossil RTI, suggest that the last phase of spreading in the Solea spreading axis formed an oceanic core complex.

The spreading rate of the Troodos fossil spreading center is a subject of some dispute. Allerton and Vine (1987, 1991) argued for fast spreading, but most other studies suggested slow-spreading environment for the Troodos ophiolite (Varga and Moores, 1985; Hurst et al., 1994; Varga et al., 1999; Cann et al., 2001). Notwithstanding this dispute there is a broad agreement that the Solea extinct spreading axis marks a phase of amagmatic spreading (Allerton and Vine, 1991; Hurst et al., 1994), which implies that the Solea axis is a relict of a slow- to intermediate-spreading axis. The Amiandos fault (AF) together with the inferred structure of oceanic core complex, are part of the slow-spreading system of the Solea extinct spreading axis. The occurrence of a fossil-OCC in the Solea axis is compatible with the present day setting of OCC at slow- (Escartin et al., 2008; Tucholke et al., 2008) to intermediate-spreading centers (Okino et al., 2004).

4.5.1. Slip history along the Amiandos Fault (AF) in the fossil spreading center

Given the southward extrapolation of the Solea spreading axis through the gabbro suite parallel to the strike of the adjacent dikes (Abelson et al., 2002), the AF is located 2 km west of the spreading axis (Fig. 1). Along the present day detachment fault of the TAG area in the Mid-Atlantic Ridge serpentinized ultramafic rocks were exhumed to a depth of 1 to 3 km at 2 km off-axis location (deMartin et al., 2007). On Troodos oceanic serpentinites that formed at 110°–180 °C occur 2 km away from the paleo-spreading axis along the AF. Therefore, both isotope thermometry and comparison with the sub-seafloor geometry of a present day OCC suggest that serpentinization has occurred at shallow crustal levels during the latest stages of the AF activity. It follows that most of the uplift accommodated along the AF had occurred prior to the serpentinization at ~2 km depth. This is supported by isotope ratios in gabbros from the vicinity of the AF, which record water–rock interaction at much lower water/rock ratios and at higher temperatures relative to the serpentinites juxtaposed against them, hence indicating a deeper and earlier stage in the AF slip. The level where the ultramafic rocks resided prior to exhumation can also be roughly constrained. The continuity of the gabbro suite and the absence of sheeted dikes directly overlying ultramafic rocks suggest that a 'plum–pudding' structure (Cannat, 1996; Ildefonse et al., 2007), i.e., a patchy distribution of gabbro intrusions within ultramafics, cannot account for Troodos oceanic crust. It is thus more likely that the ultramafic rocks were uplifted from the upper mantle.

Highly rotated (dip<50°) blocks of sheeted dikes overlie a detachment fault along the western side of the Solea extinct spreading axis (Fig. 1, Hurst et al., 1994). Detachment faults associated with overlying rotated blocks occur in spreading environments where tectonic spreading dominates over magmatism, such as 2nd-order segment edges or RTIs (e.g. Smith et al., 2008; Tucholke et al., 2008). The evolution of OCCs involves flattening of the steeply-dipping fault by an isostatic response to the thinning of the lithosphere (Buck, 1988). Therefore, the activity on the steep AF fault as well as hydrothermal alteration along the AF preceded block rotation above the detachment. This is supported by the paleomagnetic data of Varga et al. (1999) showing that the 'bookshelf' block rotation in the sheeted dike complex has occurred subsequent to epidotization, suggesting hydrothermal alteration prior to block rotation. Both products of hydrothermal discharge associated with axis-parallel faulting, i.e. epidotization of the upper crust (300–370 °C; Schiffman et al., 1987) and alteration of the AF-related gabbros of the lower crust (~500 °C; samples T-7, AF-4, AF-12), demonstrate early stages of tectonic evolution of the spreading axis (Fig. 8A and B). During later stages of the tectonic spreading, isostatic uplift due to lithospheric thinning

induced rotation of the normal faults, hence forming a flat detachment fault and block rotation (e.g. Buck, 1988; Tucholke et al., 1998; Escartin et al., 2003). This process involved further uplift of ultramafic rocks along the AF, which in turn were serpentinized in shallower depths.

4.5.2. Type of the Troodos fossil oceanic core complex (OCC)

It is difficult to determine whether the deep-seated rocks were denuded onto the seafloor by the operation of the OCC, a process that should involve uplift accommodated by the AF and additional crustal thinning by block rotation in the upper crust. The width of the off-axis structure comprising the highly rotated dikes and the AF is less than 20 km, and rotated dike blocks are in close vicinity to the Solea spreading axis. Therefore, it is reasonable to suggest a short lived system of core complex formation, with rafted blocks that did not involve exposure of gabbros and serpentinites on the seafloor. The exhumed deeply-sourced rocks were probably covered by tilted blocks of upper crust (Fig. 8B) in a similar fashion to the OCC that was recently discovered in the Mid-Atlantic Ridge around the 13°N segment (Smith et al., 2008). Furthermore, the isotope data from the AF, indicating that discharged fluids were focused into the major fault, imply the existence of an OCC at its early stages. Such channeling of hydrothermal fluids through the OCC major fault was recently observed in the TAG area (deMartin et al., 2007; McCaig et al., 2007) and in the Atlantis Massif (30°N) at the Mid-Atlantic Ridge (Delacour et al., 2008).

4.5.3. Serpentinization during ophiolite emplacement

A more pervasive serpentinization process at lower temperatures giving higher $\delta^{18}O$ values prevails both away from and close to the AF, and is characterized by fully serpentinized rocks with abundant chrysotile-filled cracks occur. The high $\delta^{18}O$ values of the chrysotile-rich serpentinite are typical of ophiolitic serpentine (Fig. 5), thus probably represent later serpentinization during emplacement of the Troodos ophiolite. The major carrier of the high $\delta^{18}O$ signature is the crack-filling chrysotile that attains its highest abundance at the heart of the highly-serpentinized domain in the Troodos massif, not far from the AF. Therefore, products of later serpentinization have precipitated in uplift-induced cracks that could have formed during the initial OCC uplift and highlighted during final ophiolite emplacement. Furthermore, the displacement of ultramafic rocks to a shallower position within an area that was topographically higher than its surroundings during the formation of the OCC in the spreading environment, could have assisted the final denudation of the ultramafic domain during the uplift phase of ophiolite emplacement (Fig. 8C).

5. Conclusions

Petrographic observations and stable isotope compositions in the serpentinized ultramafic section exposed at the Troodos RTI indicate sequential alteration events at variable tectonic settings. Early serpentinization occurred during seafloor spreading at temperatures of 110–180 °C and is associated with a major ridge axis-parallel fault. A later serpentinization event most probably occurred in an emplacement-related environment at very low-temperatures and involved intense deformation and chrysotile veining.

Subseafloor hydrothermal alteration of the gabbro suite is spatially variable. Within the AF zone, open-system alteration processes at various temperatures are evident. However, adjacent to the extinct spreading center, enhanced alteration processes occurred at amphibolite facies conditions (500–600 °C) implying on-axis hydrothermal system. The Amiandos fault thus played an important role in the off-axis hydrothermal processes in both the gabbro and the ultramafic sections. In the gabbro, alteration processes were initiated at relatively high temperatures, however, serpentinization of the ultramafic rocks occurred at lower temperatures and shallower levels. These results suggest that long-lived activity occurred along the AF during oceanic

spreading, uplifting progressively deeper parts of the oceanic lithosphere and resulting in water–rock interaction at decreasing temperatures.

The observation that 'oceanic type' serpentinites are associated with the fault zone, suggests that AF was active during oceanic spreading at the Cretaceous. Since the serpentinite exposure on Troodos occurs in a ridge–transform intersection along an oceanic fault that is parallel to the spreading axis, a fossil core complex scenario, or at least a juvenile structure of core complex should be considered. This model is supported by the fact that the western side of the Solea graben was extensively stretched, as indicated by the book-shelf block rotation above a detachment fault conjugated with the AF. Removal of the upper oceanic layers by a long-lived detachment fault, and the consequent isostatic uplift, could have resulted in denudation of mantle rocks to shallow levels within the oceanic crust. This denudation was accompanied by the rotation of the rafted blocks as interpreted from the currently active Mid-Atlantic Ridge near 13°N. This scenario occurs where tectonic spreading becomes dominant over magmatic spreading, in agreement with the location at the segment edge, i.e., the Troodos fossil RTI.

Appendix A. Supplementary data

Supplementary data associated with this article can be found, in the online version, at doi:10.1016/j.epsl.2009.02.029.

References

Abelson, M., Baer, G., Agnon, A., 2001. Evidence from gabbro of the Troodos ophiolite for lateral magma transport along a slow-spreading mid-ocean ridge. Nature 409, 72–75.

Abelson, M., Baer, G., Agnon, A., 2002. Fossil ridge–transform intersection in the Troodos ophiolite: new perspectives from rock magnetism in the gabbro suite and fracture mechanics analysis. Geochem. Geophys. Geosyst. 3. doi:10.1029/2001GC000245.

Agrinier, P., Hékinian, R., Bideau, D., Javoy, M., 1995. O and H stable isotope compositions of oceanic crust and upper mantle rocks exposed in the Hess Deep near the Galapagos Triple Junction. Earth Planet. Sci. Lett. 136, 183–196.

Allerton, S., 1989. Distortions, rotation and crustal thinning at ridge–transform intersections. Nature 340, 626–628.

Allerton, S., Vine, F.J., 1987. Spreading structure of the Troodos ophiolite, Cyprus; some paleomagnetic constraints. Geology 15, 593–597.

Allerton, S., Vine, F.J., 1991. Spreading evolution of the Troodos ophiolite, Cyprus. Geology 19, 637–640.

Andreani, M., Mevel, C., Boullier, A.M., Escartin, J., 2007. Dynamic control on serpentine crystallization in veins; constraints on hydration processes in oceanic peridotites. Geochem. Geophys. Geosyst. 8. doi:10.1029/2006GC001373.

Bickle, M.J., Teagle, D.A.H., Beyon, J., Chapman, H.J., 1998. The strcture and controls on fluid–rock interactions in ocean ridge hydrothermal systems: constraints from the Troodos ophiolite. In: Mills, R.A., Harrison, K. (Eds.), Modern Ocean Floor Processes and the Geological Record. Geol. Soc. Spec. Publ. London, pp. 127–152.

Bishopp, D.W., Wilson, R.A.M., Burdon, D.J., Carr, J.M., 1978. Geological map of the Xeros–Troodos area. Cyprus Geological Survey Department.

Blackmann, D.K., Cann, J.R., Janssen, B., Smith, D.K., 1998. Origin of extensional core complexes: evidence from the Mid-Atlantic Ridge at the Atlantis Fracture Zone. J. Geophys. Res. 103, 21315–21333.

Boronina, A., Balderer, W., Renard, P., Stichler, W., 2005. Study of stable isotopes in the Kouris catchment (Cyprus) for the description of the regional groundwater flow. J. Hydrol. 308, 214–226.

Boschi, C., Dini, A., Früh-Green, G.L., Kelley, D.S., 2008. Isotopic and element exchange during serpentinization and metasomatism at the Atlantis Massif (MAR 30°N): insights from B and Sr isotope data. Geochim. Cosmochim. Acta 72, 1801–1823.

Buck, W.R., 1988. Flexural rotation of normal faults. Tectonics 7, 959–973.

Cann, J.R., Blackman, D.K., Smith, D.K., McAllister, E., Janssen, B., Mello, S., Avgerinos, E., Pascoe, A.R., Escartin, J., 1997. Corrugated slip surfaces formed at ridge–transform intersections on the Mid-Atlantic Ridge. Nature 385, 329–332.

Cann, J.R., Prichard, H.M., Malpas, J., Xenophontos, C., 2001. Oceanic inside corner detachments of the Limassol Forest area, Troodos ophiolite, Cyprus. J. Geol. Soc. Lond. 158, 757–767.

Cannat, M., 1993. Emplacement of mantle rocks in the seafloor at mid-ocean ridges. J. Geophys. Res. 98, 4163–4172.

Cannat, M., 1996. How thick is the magmatic crust at slow spreading oceanic ridges? J. Geophys. Res. B: Solid Earth 101, 2847–2857.

Cannat, M., Mevel, C., Maia, M., Deplus, C., Gente, P., Agrinier, P., Belarouchi, A., Dubuisson, G., Humler, E., Reynolds, J., 1995. Thin crust, ultramafic exposures, and rugged faulting patterns at the Mid-Atlantic Ridge (22–24°N). Geology 23, 49–52.

Clayton, R.N., Goldsmith, J.R., Mayeda, T.K., 1989. Oxygen isotope fractionation in quartz, albite, anorthite and calcite. Geochim. Cosmochim. Acta 53, 725–733.

Delacour, A., Früh-Green, G.L., Frank, M., Gutjahr, M., Kelley, D.S., 2008. Sr- and Nd-isotope geochemistry of the Atlantis Massif (30°N, MAR): implications for fluid fluxes and lithospheric heterogeneity. Chem. Geol. 254, 19–35.

deMartin, B.J., Sohn, R.A., Canales, J.P., Humphris, S.E., 2007. Kinematics and geometry of active detachment faulting beneath the Trans-Atlantic Geotraverse (TAG) hydro-thermal field on the Mid-Atlantic Ridge. Geology 35, 711–714.

Demény, A., 1994. H isotope fractionation due to hydrogen–zinc reactions and its implications on D/H analysis of water samples. Chem. Geol. 121, 19–25.

Dipple, G.M., Ferry, J.M., 1992. Fluid flow and stable isotopic alteration in rocks at elevated temperatures with applications to metamorphism. Geochim. Cosmochim. Acta 56, 3539–3550.

Escartin, J., Mevel, C., MacLeod, C.J., McCaig, A.M., 2003. Constraints on deformation conditions and the origin of oceanic detachments: the Mid-Atlantic Ridge core complex at 15° 45′N. Geochem. Geophys. Geosyst. 4. doi:10.1029/2002GC000472.

Escartin, J., Smith, D.K., Cann, J., Schouten, H., Langmuir, C.H., Escrig, S., 2008. Central role of detachment faults in accretion of slow-spreading oceanic lithosphere. Nature 455, 790–794.

Evans, B.W., Johannes, W., Oterdoom, H., Trommsdorff, V., 1976. Stability of chrysotile and antigorite in the serpentine multisystem. Schweiz. Mineral. Petrogr. Mitt. 56, 79–93.

Ferry, J.M., 1986. Reaction Progress; a Monitor of Fluid–Rock Interaction During Metamorphic and Hydrothermal Events. Springer-Verlag, New York, NY.

Früh-Green, G.L., Kelley, D.S., Bernasconi, S.M., Karson, J.A., Ludwig, K.A., Butterfield, D.A., Boschi, C., Proskurowski, G., 2003. 30,000 years of hydrothermal activity at the Lost City vent field. Science 301, 495–498.

Gass, I.G., 1990. Ophiolites and oceanic lithosphere. In: Malpas, J., Moores, E.M., Panayiotou, A., Xenophontos, C. (Eds.), Ophiolites, Oceanic Crustal Analogues, Proc. Symp. 'Troodos 1987'. Cyprus Geological Survey Department, Nicosia, pp. 1–12.

Gillis, K., 1995. Controls on hydrothermal alteration in a section of fast-spreading oceanic crust. Earth Planet. Sci. Lett. 134, 473–489.

Gillis, K., Roberts, M.D., 1999. Cracking at the magma–hydrothermal transition: evidence from the Troodos Ophiolite, Cyprus. Earth Planet. Sci. Lett. 169, 227–244.

Granot, R., Abelson, M., Ron, H., Agnon, A., 2006. The oceanic crust in 3D: Paleomagnetic reconstruction in the Troodos ophiolite gabbro. Earth Plant. Sci. Lett. 251, 280–292. doi:10.1016/j.epsl.2006.09.019.

Gregory, R.T., Criss, R.E., Taylor, H.P., 1989. Oxygen isotope exchange kinetics of mineral pairs in closed and open systems: applications to problems of hydrothermal alteration of igneous rocks and Precambrian iron formations. Chem. Geol. 75, 1–42.

Gregory, R.T., Taylor, H.P., 1981. An oxygen isotope profile in a section of Cretaceous oceanic crust, Semail ophiolite, Oman: evidence for $\delta^{18}O$ buffering of the oceans by deep (>5 km) seawater–hydrothermal circulation at mid-ocean ridges. J. Geophys. Res. 86, 2737–2755.

Heaton, T.H.E., Sheppard, S.M.F., 1977. Hydrogen and oxygen isotope evidence for sea-water–hydrothermal alteration and ore deposition, Troodos complex, Cyprus. Volcanic Processes in Ore Genesis. Geol. Soc. Spec. Publ., 7, London, pp. 42–57.

Humphris, S.E., Cann, J.R., 2000. Constraints on the energy and chemical balances of the modern TAG and ancient Cyprus seafloor sulfide deposits. J. Geophys. Res. B: Solid Earth 105, 28477–28488.

Hurst, S.D., Karson, J.A., Moores, E.M., 1990. Nodal basins at slow spreading ridge–transform intersections: a comparison to the central portion of the Troodos ophiolite. In: Malpas, J., Moores, E.M., Panayiotou, A., Xenophonotos, C. (Eds.), Ophiolites, Oceanic Crustal Analogues, Proc. Symp. 'Troodos 1987'. Cyprus Geological Survey Department, Nicosia, pp. 125–130.

Hurst, S.D., Moores, E.M., Varga, R.J., 1994. Structural and geophysical expression of the Solea graben, Troodos Ophiolite, Cyprus. Tectonics 13, 139–156.

Ildefonse, B., Blackman, D.K., John, B.E., Ohara, Y., Miller, D.J., MacLeod, C.J., 2007. Oceanic core complexes and crustal accretion at slow-spreading ridges. Geology 35, 623–626.

Karson, J.A., Thompson, G., Humphris, S.E., Edmonds, J.M., Bryan, W.B., Brown, J.R., Winters, A.T., Pockalny, R.A., Casey, J.F., Campbell, A.C., Klinkhammer, G., Palmer, M.R., Kinzler, R.J., Sulanowska, M.M., 1987. Along axis variation in seafloor spreading in the MARK area. Nature 328, 681–685.

Kelley, D.S., Robinson, P.T., 1990. Development of a brine-dominated hydrothermal system at temperatures of 400–500 °C in the upper level plutonic sequence, Troodos ophiolite, Cyprus. Geochim. Cosmochim. Acta 54, 653–661.

Kelley, D.S., Karson, J.A., Fruh-Green, G.L., Yoerger, D.R., Shank, T.M., Butterfield, D.A., Hayes, J.M., Schrenk, M.O., Olson, E.J., Proskurowski, G., Jakuba, M., Bradley, A., Larson, B., Ludwig, K., Glickson, D., Buckman, K., Bradley, A.S., Brazelton, W.J., Roe, K., Elend, M.J., Delacour, A., Bernasconi, S.M., Lilley, M.D., Baross, J.A., Summons, R.E., Sylva, S.P., 2005. A serpentinite-hosted ecosystem: the Lost City Hydrothermal Field. Science 307, 1428–1434.

Kohn, M.J., Valley, J.W., 1998. Oxygen isotope geochemistry of the amphiboles: isotope effects of cation substitutions in minerals. Geochim. Cosmochim. Acta 62, 1947–1958.

Kyser, T.K., Kerrich, R., 1991. Retrograde exchange of hydrogen isotopes between hydrous minerals and water at low temperatures. In: Taylor, H.P., O'Neil, J.R., Kalpan, I.R. (Eds.), Stable Isotope Geochemistry: a Tribute to Samual Epstein. Geochem. Soc. Spec. Publ., 3, pp. 409–424.

MacLeod, C.J., Allerton, S., Gass, I.G., Xenophonotos, C., 1990. Structure of a fossil ridge–transform intersection in the Troodos ophiolite. Nature 348, 717–720.

MacLeod, C.J., Escartin, J., Banerji, D., Banks, G.J., Gleeson, M., Irving, D.H.B., Lilly, R.M., McCaig, A.M., Niu, Y., Allerton, S., Smith, D.K., 2002. Direct geological evidence for oceanic detachment faulting: the Mid-Atlantic Ridge, 15°45′N. Geology 30, 879–882.

Magaritz, M., Taylor, H.P.J., 1974. Oxygen and hydrogen isotope studies of serpentiniza-tion in the Troodos ophiolite complex, Cyprus. Earth Planet. Sci. Lett. 23, 8–14.

Malpas, J., 1990. Accretionary processes in the Troodos ophiolite, Cyprus: evidence from field mapping and deep crustal drilling. In: Malpas, J., Moores, E.M., Panayiotou, A., Xenophontos, C. (Eds.), Ophiolites, Oceanic Crustal Analogues, Proc. Symp. 'Troodos 1987'. Cyprus Geological Survey Department, Nicosia, pp. 65–74.

Malpas, J., Brace, T., 1987. The geology of Pano–Amiandos–Palekhori area, Cyprus. 1:125000 map. Cyprus Geolgical Survey Department.

Mattey, D., Lowry, D., Macpherson, C., 1994. Oxygen isotope composition of mantle peridotite. Earth Planet. Sci. Lett. 128, 231–241.

Matthews, A., Goldsmith, J.R., Clayton, R.N., 1983. Oxygen isotope fractionations involving pyroxenes: the calibration of mineral-pair geothermometers. Geochim. Cosmochim. Acta 47, 631–644.

McCaig, A.M., Cliff, R.A., Escartin, J., Fallick, A.E., MacLeod, C.J., 2007. Oceanic detachment faults focus very large volumes of black smoker fluids. Geology 35, 935–938.

Mével, C., 2003. Serpentinization of abyssal peridotites at Mid-ocean ridges. Geoscience 335, 825–852.

Mével, C., Cannat, M., Gente, P., Marion, E., Auzende, J.M., Karson, J.A., 1991. Emplacement of deep crustal and mantle rocks on the west median valley wall of the MARK area (MAR, 23°N). Tectonophysics 190, 31–53.

Nicolas, A., Boudier, F., 1995. Mapping oceanic ridge segments in Oman ophiolite. J. Geophys. Res. 100, 6179–6197.

O'Hanley, D.S., 1996. Serpentinites: Records of Tectonic and Petrological History. Oxford university press, New York.

Okino, K., Matsuda, K., Christie, D.M., Nogi, Y., Koizumi, K.-i., 2004. Development of oceanic detachment and asymmetric spreading at the Australian–Antarctic discordance. Geochem. Geophys. Geosyst. 5. doi:10.1029/2004GC000793.

Proskurowski, G., Lilley, M.D., Kelley, D.S., Olson, E.J., 2006. Low temperature volatile production at the Lost City Hydrothermal Field, evidence from a hydrogen stable isotope geothermometer. Chem. Geol. 229, 331–343.

Putlitz, B., Matthews, A., Valley, J.W., 2000. Oxygen and hydrogen isotope study of high-pressure metagabbros and metabasalts (Cyclades, Greece): implications for the subduction of oceanic crust. Contrib. Mineral. Petrol. 138, 114–126.

Reston, T.J., Weinrebe, W., Grevemeyer, I., Flueh, E.R., Mitchell, N.C., Kirstein, L., Kopp, C., Kopp, H., 2002. A rifted inside corner massif on the Mid-Atlantic Ridge at 5°S. Earth Planet. Sci. Lett. 200, 255–269.

Sakai, R., Kusakabe, M., Noto, M., Ishii, T., 1990. Origin of waters responsible for serpentinization of the Izu–Ogasawara–Mariana forearc seamounts in view of hydrogen and oxygen isotope ratios. Earth Planet. Sci. Lett. 100, 291–303.

Schiffman, P., Smith, B.M., Varga, R.J., Moores, E.M., 1987. Geometry, conditions and timing of off-axis hydrothermal metamorphism and ore-deposition in the Solea graben. Nature 325, 423–425.

Sheppard, S.M.F., 1980. Isotopic evidence for the origins of water during metamorphic processes in oceanic crust and ophiolite complexes. Coll. Int. C.N.R.S 272, 135–147.

Simonian, K.O., Gass, I.G., 1978. Arakapas fault belt, Cyprus: a fossil transform fault. Geol. Soc. Amer. Bull. 89, 1220–1230.

Smith, D.K., Escartín, A.J., Schouten, A.H., Cann, A.J.R., 2008. Fault rotation and core complex formation: significant processes in seafloor formation at slow-spreading mid-ocean ridges (Mid-Atlantic Ridge, 13°–15°N). Geochem. Geophys. Geosyst. 9. doi:10.1029/2007GC001699.

Spicuzza, M.J., Valley, J.W., McConnell, V.S., 1998. Oxygen isotope analysis of whole rocks via laser-fluorination: an air-lock approach. Geol. Soc. Am. Abs. Prog. 30, 80.

Stakes, D., 1991. Oxygen and hydrogen isotope composition of oceanic plutonic rocks: high-temperature deformation and metamorphism of oceanic layer 3. In: Taylor, H.P.J., O'Neil, J.R., Kalpan, I.R. (Eds.), Stable Isotope Geochemistry: a Tribute to Samuel Epstein. Geochem. Soc. Spec. Publ. 3 , pp. 77–90.

Taylor, H.P.J., 1977. Water/rock interactions and the origin of H$_2$O in granitic batholiths. J. Geol. Soc. Lond. 133, 509–558.

Tucholke, B.E., Behn, M.D., Buck, W.R., Lin, J., 2008. Role of melt supply in oceanic detachment faulting and formation of megamullions. Geology 36, 455–458.

Tucholke, B.E., Fujioka, K., Ishihara, T., Hirth, G., Kinoshita, M., 2001. Submersible study of an oceanic megamullion in the central North Atlantic. J. Geophys. Res. 106, 16145–16161.

Tucholke, B.E., Lin, J., Kleinrock, M.C., 1998. Megamullions and mullion structure defining oceanic metamorphic core complexes on the Mid-Atlantic Ridge. J. Geophys. Res. B: Solid Earth 103, 9857–9866.

Valley, J.W., Kitchen, N., Kohn, M.J., Niendorf, C.R., Spicuzza, M.J., 1995. UWG-2, a garnet standard for oxygen isotope ratios: strategies for high precision and accuracy with laser heating. Geochim. Cosmochim. Acta 59, 5223–5231.

Varga, R.J., Moores, E.F., 1985. Spreading structure of the Troodos ophiolite, Cyprus. Geology 13, 846–850.

Varga, R.J., Gee, J.S., Bettison-Varga, L., Anderson, R.S., Johnson, C.L., 1999. Early establish-ment of seafloor hydrothermal systems during structural extension: paleomagnetic evidence from the Troodos ophiolite, Cyprus. Earth Planet. Sci. Lett. 171, 221–235.

Vennemann, T.W., O'Neil, J.R., 1993. A Simple and inexpensive method of hydrogen isotope and water analyses of minerals and rocks based on zinc reagent. Chem. Geol. 103, 227–234.

Wenner, D.B., Taylor, H.P.J., 1971. Temperature of serpentinization of ultramafic rocks based on 18O/16O fractionation between coexisting serpentine and magnetite. Contrib. Mineral. Petrol. 32, 165–185.

Wenner, D.B., Taylor, H.P.J., 1973. Oxygen and hydrogen isotope studies of the serpentinization of ultramafic rocks in the oceanic environment and continental ophiolite complexes. Am. J. Sci. 273, 207–239.

Wernicke, B.P., 1992. Interpretive tectonic map showing known areas of strong upper crustal extension and regional topography. Geol. Soc. Amer. G3.

Wicks, F.J., Whittaker, E.J.W., 1977. Serpentine textures and serpentinization. Cana. Mineralogist 15, 459–488.

Zheng, Y.F., Metz, P., Satir, M., 1994. Oxygen isotope fractionation between calcite and tremolite: an experimental study. Contrib. Mineral. Petrol. 118, 249–255.